

PAPER

## Sub-picosecond pulsed THz FET detector characterization in plasmonic detection regime based on autocorrelation technique

To cite this article: K Ikamas *et al* 2018 *Semicond. Sci. Technol.* **33** 124013

View the [article online](#) for updates and enhancements.






**IOP | ebooks™**

Bringing you innovative digital publishing with leading voices to create your essential collection of books in STEM research.

Start exploring the collection - download the first chapter of every title for free.

# Sub-picosecond pulsed THz FET detector characterization in plasmonic detection regime based on autocorrelation technique

K Ikamas<sup>1,2</sup>, A Lisauskas<sup>1</sup> , S Massabeau<sup>3</sup>, M Bauer<sup>4,6</sup>, M Burakevič<sup>1</sup>, J Vyšniauskas<sup>1</sup>, D Čibiraite<sup>4</sup> , V Krozer<sup>4,5</sup>, A Rämmer<sup>5</sup>, S Shevchenko<sup>5</sup>, W Heinrich<sup>5</sup>, J Tignon<sup>3</sup>, S Dhillon<sup>3</sup>, J Mangeney<sup>3</sup> and H G Roskos<sup>4</sup> 

<sup>1</sup>Institute of Applied Electrodynamics and Telecommunications, Vilnius University, 10257 Vilnius, Lithuania

<sup>2</sup>General Jonas Žemaitis Military Academy of Lithuania, Šilo str. 5A, LT-10322 Vilnius, Lithuania

<sup>3</sup>Laboratoire Pierre Aigrain, Ecole Normale Supérieure-PSL Research University, CNRS, Université Pierre et Marie Curie-Sorbonne Universités, Université Denis Diderot-Sorbonne Paris Cité, 24 rue Lhomond, F-75231 Paris Cedex 05, France

<sup>4</sup>Physikalisches Institut, Goethe Universität Frankfurt, D-60438 Frankfurt, Germany

<sup>5</sup>Ferdinand-Braun-Institut, Leibniz Institut für Höchstfrequenztechnik, D-12489 Berlin, Germany

<sup>6</sup>Center for Materials Characterization and Testing, Fraunhofer ITWM, D-67663 Kaiserslautern, Germany

E-mail: [alvydas.lisauskas@ff.vu.lt](mailto:alvydas.lisauskas@ff.vu.lt)

Received 24 July 2018, revised 28 September 2018

Accepted for publication 17 October 2018

Published 7 November 2018



CrossMark

## Abstract

Many THz applications require detection of sub-picosecond THz pulses. Electronic detectors, in particular, can address this challenge. We report on the detection of sub-picosecond THz pulses generated by a large-area interdigitated photoconductive antenna using a AlGa<sub>N</sub>/Ga<sub>N</sub> high electron mobility transistor with integrated bow-tie antenna. We demonstrate that the detector's photoresponse is linear in a wide range of gate bias voltages regarding the available THz radiation power with peak power levels of a few hundreds of milliwatts. We apply an autocorrelation technique to investigate the spectral response of our detector within a bandwidth exceeding 1 THz. We observe an unexpected frequency roll-off of responsivity, which can not be predicted using a framework of standard distributed transmission line theory. However, we show that the data can be understood if one accounts for only partial plasmon screening by the gate electrode, so that the results adhere simply to the distributed resistive mixing approximation, whereby the device suffers from the observed roll-off. This indicates, that for novel detectors and radiation sources, which intend to utilize plasma waves, it is important to ensure efficient screening by the gate electrode.

Keywords: field-effect transistor, rectification, submillimeter waves, plasma wave detector, terahertz detector

(Some figures may appear in colour only in the online journal)

## 1. Introduction

The autocorrelation technique is a common method which can be applied over the whole electromagnetic spectrum, from UV and visible light down to infrared and terahertz (THz) frequencies. In general, two types of detectors can be employed—linear or nonlinear to the incident radiation

power. Antenna-coupled field-effect transistors for THz detection (TeraFETs) have recently emerged as practical devices for THz autocorrelators [1, 2]. By now, many different types of FETs were shown to be efficient THz detectors including high-electron-mobility transistors (HEMTs) [3], complementary metal-oxide semiconductor (CMOS) FETs [4], nanowire-based transistors in a 1D configuration [5] or

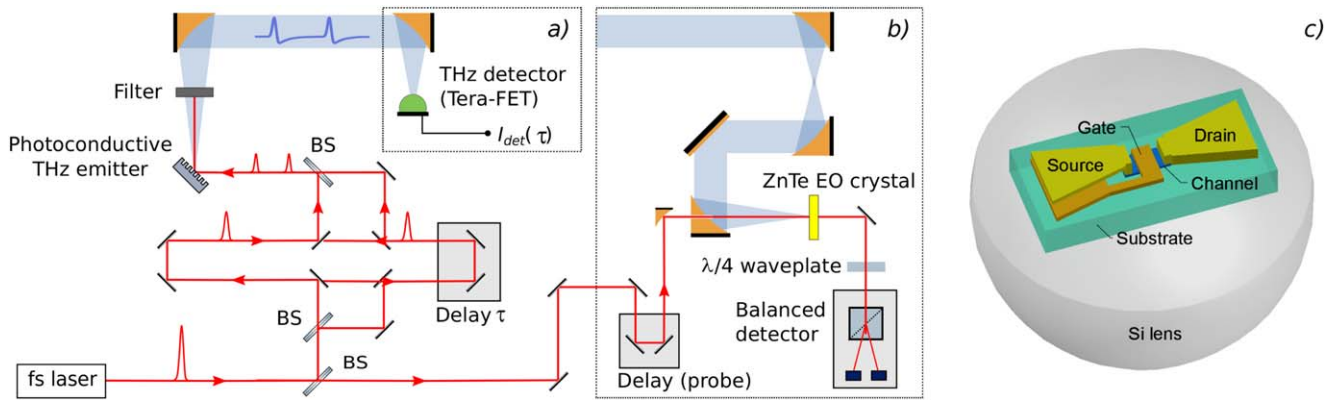


**Figure 1.** (a) The setup for characterization of AlGaIn/GaN TeraFET detector response and autocorrelation measurements. (b) The setup for reference autocorrelation and time-domain measurements with an electro-optical detector (ZnTe crystal). The power of the emitted THz radiation is modulated by biasing the antenna of the photoconductive emitter with a square wave signal (not shown in diagram). The response of the TeraFET detector is measured using a lock-in amplifier (also omitted in diagram). (c) A simplified detector's schematic view. Details are not to scale.

graphene FETs [6–8]. The detection principle is based on a combination of plasma wave-influenced mixing [4, 9] and thermoelectric signals [6–8, 10, 11] in the FET's channel. State-of-the-art FETs show high responsivity (up to 1000 V/W), low noise equivalent power (down to 30 pW Hz<sup>-1/2</sup>) [12] and fast response time (shorter than 30 ps [13]).

At weak radiation power levels, TeraFETs are operated as linear detectors, i.e. the observed photoresponse is linear in radiation intensity [14]. However, for high excitation levels, Schottky diodes and FETs can be driven into saturation [15–17]. Recently, the application of this device regime for fast autocorrelators providing information on the THz pulse duration and pulse structure [1, 18] was reported.

Here, we report on the efficient autocorrelation measurement of sub-picosecond THz pulses generated by an ultrafast large-area interdigitated photoconductive antenna with a broadband field-effect transistor. As it was mentioned above, there are multiple of choices for material system to be used for the implementation of the detector. We focus on broadband antenna-coupled AlGaIn/GaN HEMT which, in the vicinity of 600 GHz, provides with record reported sensitivities (relating to the available power in the beam). Only recently the sensitivity of our AlGaIn/GaN devices above 1 THz was surpassed by a CMOS TeraFET [19]. The technique presented here is independent on the choice of the detector and can be exploited to perform fast autocorrelation characterizations of a variety of THz detectors and low power THz photomixers. Additionally, we concentrate on the study of peculiarities of the broadband THz response in the so-called plasmonic rectification regime predicted by the theoretical works of Dyakonov and Shur [9].

The paper is organized in the following way: in section 2 we provide the detailed information about the experimental setup and AlGaIn/GaN detector. Section 3 is dedicated for experimental findings, followed by theory in section 4, and later on discussion and summary.

## 2. Experiment setup

Figure 1(a) presents a measurement setup which employs a Ti:sapphire laser coupled to a nonlinear fiber for generation of infrared radiation pulses with 15–47 fs duration. This setup was a part of a diffraction-limited THz time-domain spectroscopy system (THz-TDS) [20, 21]. A 45 fs duration, 80 MHz repetition rate pulse train centered at a wavelength of 800 nm from a Ti:sapphire oscillator system is chirped and compressed down to 20 fs long pulses. The energy of compressed pulses reach up to 4 nJ. In order to perform autocorrelation measurements, the beam is separated into two optical paths, one of them is delayed with a mechanical stage. Then both arms are overlapped and guided to a large-area interdigitated photoconductive antenna. The antenna consists of metallic electrodes with 2 μm width and 2 μm spacing patterned on a 1 μm thick low-temperature grown GaAs material on semi-insulating GaAs wafer. The metal–semiconductor–metal finger structure is masked every second period by a second metalization (Cr–Au), ensuring the generation of only in-phase radiation [22]. The second metalization is isolated from the first by a SiO<sub>2</sub> layer of 560 nm thickness. The antenna surface is 500 × 500 μm<sup>2</sup>. When screening processes [23, 24] in the THz emitter are sufficiently low, the two optical pump pulses generate two independent, identical THz pulses with variable delay. This was confirmed by control measurements of the THz fields (and emitter DC currents) versus optical pump power which will be discussed further in the text.

The emitter is biased by 0–10 V peak-to-peak square wave with 13 kHz modulation frequency. The measurable bandwidth of the TDS system can reach up to 14.5 THz with the spectra maximum at approximately 1.5 THz [20]. The emitted THz radiation is first collimated and then focused using two off-axis parabolic mirrors onto the TeraFET. The additional polytetrafluorethylen sheet is placed into the beam between the parabolic mirrors to block the residual infrared radiation. A response of the detector is measured using a lock-in technique.

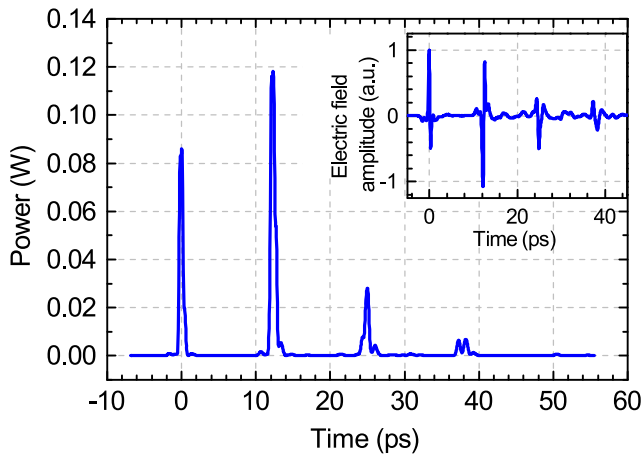


**Figure 2.** The peaks power calculated from the time-domain measurements with electro-optical detector. The one THz pulse contains several peaks with a temporal delay of 12.5 ps which originate from the internal reflections in a photomixer emitter. The inset shows the shape of the pulse.

We used a bow-tie antenna-coupled THz detector based on AlGaIn/GaN HEMT [3]. Figure 1(c) depicts a simplified device's schematic view. Transistor has a 100 nm long gate ( $L_{\text{ch}}$ ), the gate width ( $W$ ) is  $3 \mu\text{m}$ , the gate-to-channel separation ( $d$ ) is 14 nm and the length of two equally-long ungated regions is 300 nm. It was fabricated in a GaN MMIC process on SiC substrate at Ferdinand-Braun-Institute (FBH, Germany). A hyper-hemispherical silicon substrate lens is used to enhance coupling of THz radiation. Following parameters were extracted from the measured static resistance  $R_{\text{DC}}$ : the threshold voltage is  $-0.98 \text{ V}$ , electron mobility is  $1013 \text{ cm}^2 \text{ V}^{-1} \text{ s}^{-1}$  and the part of the DC resistance, which is not controlled by the gate voltage (series resistance), is  $651 \Omega$ . The most of it (ca.  $550 \Omega$ ) originates from the ungated regions of the channel.

In order to test the bandwidth of the emitted radiation, we have performed the time-domain characterizations on both of pump beam arms using an electro-optical (EO) detector (ZnTe crystal) as it is shown in the figure 1(b). Furthermore, by fixing the time delay of the probe beam to the maximum of EO-signal we also performed the comparative autocorrelation measurements by varying the time delay between two pump beam arms.

The measured average power of terahertz radiation has been  $15 \mu\text{W}$ . The calculated peak power per one pulse has been 0.4 W. The distribution of power in one pulse is shown in the figure 2 and has been calculated using a data from time-domain measurements with EO detector and a following equation which can be derived from Poynting theorem of electrodynamics

$$P(t) = \epsilon_0 c n \int_A dS \frac{1}{T} \int_{t-T/2}^{t+T/2} E^2(t') dt', \quad (1)$$

where  $n$  is the refractive index,  $c$  is the velocity of light in vacuum,  $\epsilon_0$  is the dielectric permittivity,  $E$  is the electric field amplitude of THz radiation and the first integral stands for integration over the beam cross section. The temporal averaging is performed over one optical period  $T$ , usually replaced

by the response time of the detector. The THz emission resulting from a single laser excitation contains several peaks with a temporal delay of 12.5 ps which originate from the internal reflections in a photomixer. Note that the power of the first peak shown in the figure 2 is slightly lower than that for the second one (pulse powers of 85 mW and 120 mW, respectively). Resulting first pulse is radiated directly into free space and has widest spectrum, whereas the main power from the antenna, due to high dielectric permittivity of GaAs, goes into the substrate. It gets reflected from the bottom semiconductor/(metallic holder) interface, travels back to the front surface and gets out. Further internal reflections carry only a decreasing fraction of the power.

### 3. Results of experimental characterizations

In this section we present the results of the experimental characterization of our TeraFET based on autocorrelation technique.

#### 3.1. Linearity of the detector's response

The detection with FETs is based on the rectification of a THz voltage (or current) in the channel of the FET. In small-signal approximation, theory predicts linear response to the incident power [9, 25–27] and a square root dependence at high power radiation [28, 29]. The predictions have been validated for different material systems [15] as well as for different biasing regime [28].

Whereas pulsed THz sources that are based on either photomixing or optical rectification usually exhibit low average power levels (up to several of  $\mu\text{W}$ ), the power at the peak can reach watt levels. Therefore, we characterized the response of detector versus the power of THz radiation. For this part of the experiment we have bypassed beam splitters and delay lines in the pump beam which allowed to generate the highest available output power levels with this setup. The magnitude of THz power incident to the detector was controlled by antenna bias (see figure 3(a)) within the range for which  $P_{\text{THz}} \propto I_{\text{ph}}^2$ , where  $I_{\text{ph}}$  is a photo-generated current. We found that in the wide range of gate bias (above the threshold voltage  $V_{\text{th}} = -0.98 \text{ V}$ ), detected signal follows antenna bias amplitude to the square as expected from the linear dependence of the electric field amplitude (figure 3(b)). This confirms that TeraFET detectors operate as linear THz detectors across a large power range.

For the gate bias below the threshold voltage we have observed that the detected signal does not follow the antenna bias amplitude to the square but increases in a super-linear manner. A super-linearity and later forthcoming saturation of the response were previously observed for AlGaIn/GaN HEMT in [17]. The more detailed discussion of this phenomena is given elsewhere [18].

Therefore, we find that the linearity range of the AlGaIn/GaN TeraFET can be relatively large and for excitation with pulsed radiation it can extend over many decades reaching up to hundreds of milliwatt levels at the peak.

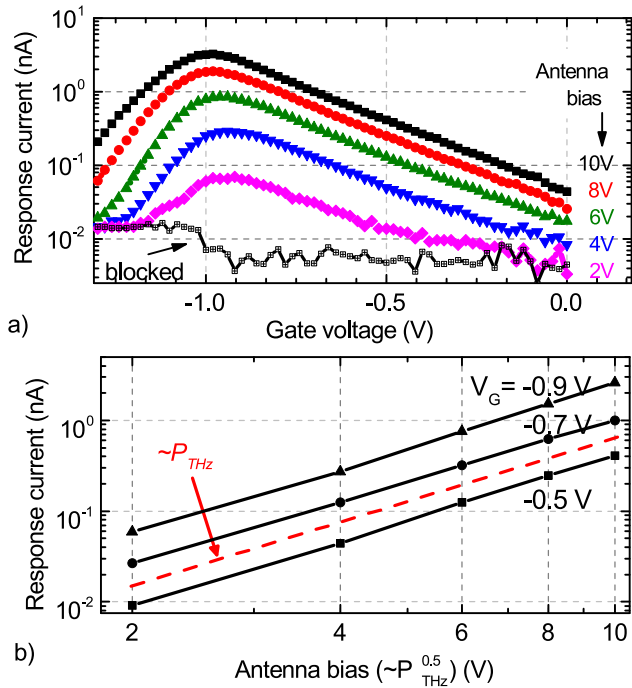


**Figure 3.** (a) Gate bias dependency of a AlGaIn/GaN HEMT current response to a pulsed THz radiation at different intensities. The radiation power is changed by applying the voltage bias between GaAs antenna's electrodes. The duration of laser pulses is 20 fs, the antenna's modulation frequency is 13 kHz. (b) The vertical cross-sections of the diagram at  $-0.5$  V,  $-0.7$  V and  $-0.9$  V of gate voltage show a linearity in the detector response. The noise ('blocked') signals is subtracted from the response. A red line is a guide to the eye.

### 3.2. Autocorrelation measurements

Figure 4(a) presents an autocorrelation trace recorded with the wide-bandwidth AlGaIn/GaN HEMT detector. The trace is symmetric, since the pulse is convoluted with itself. The measurements show a sequence of additional peaks originating from the internal reflections in a photomixer source. One of the possibilities to avoid these reflections has been recently presented in [30], which reports on the echo-less design of an interdigitated photoconductive antenna.

Figure 4(b) presents the Fourier transform of the autocorrelation trace (black solid line) measured with the TeraFET biased to  $-0.95$  V. The spectrum contains frequency components which span from 100 GHz to about 1.5 THz peaking at approx. 580 GHz. The spectrum exhibits a dip at 300 GHz. The target frequency range for the designed bow-tie antenna spans from 0.5 to 1.2 THz. Below 0.5 THz the matching between the incoming wave and the two-dimensional electron gas (2DEG) is a combination of the antenna, the thin feed line, and the ground guard ring which was originally designed to 'shield' from the influence of neighboring detectors and ensure clean analysis of devices. This leads to an impedance minimum of  $5 \Omega$  at 0.3 THz resulting to diminished power coupling in the 2DEG. Since the dip appears at the frequencies of practical interest, in the future it can be easily circumvent by different means such like extending antenna leafs, increasing the diameter of the guard ring and etc.

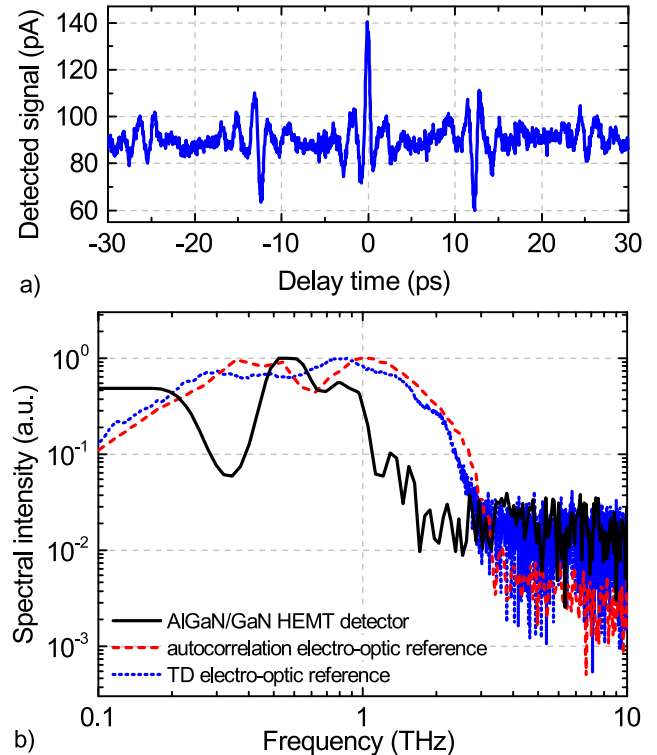


**Figure 4.** (a) Autocorrelation trace of AlGaIn/GaN HEMT response. The duration of laser pulses is 20 fs, the antenna's bias is 10 V, the modulation frequency is 13 kHz and the gate voltage of transistor is  $-0.95$  V. (b) Spectrum of the response calculated from the autocorrelation trace (solid line) and the reference spectra measured with an electro-optic detector in the same setup (dotted line) and the time-domain setup (dashed line).

The dashed line in the figure 4(b) represents the reference spectrum obtained by the same autocorrelation technique but employing a ZnTe crystal as a detector. The dotted line shows the spectrum which comes from one of the pump beams when scanning the EO-signal with the probe beam using a time-domain scanning method. Since, the pump beam was split into two, the achievable signal-to-noise ratio (SNR) was only about 100 instead of typical for TD-systems  $\approx 10^5$ . However, a direct comparison of the SNR values in equal experimental conditions show, that FET-detectors can be competitive with the EO-detectors, provided that they will be used in a heterodyne or homodyne configurations. Furthermore, we would like to note, that even in this configuration, the generated THz radiation contains enough spectral components necessary for the detector characterization.

Even with the reduced spectral bandwidth, the width of the central correlation peak can be estimated to be about 380 fs full width at half maximum. Therefore, we conclude that the TeraFET was efficiently detecting pulses of a sub-picosecond duration.

Figure 5 presents the normalized spectral characteristics. Additionally, we include two other data-sets obtained with the cw-systems: (i) an electronic multiplier-based system, tunable from 500 GHz up to 700 GHz with power levels in the order of  $100 \mu\text{W}$  allowing for calibration of detector responsivity [3, 12], and (ii) a photomixer-based system tunable from

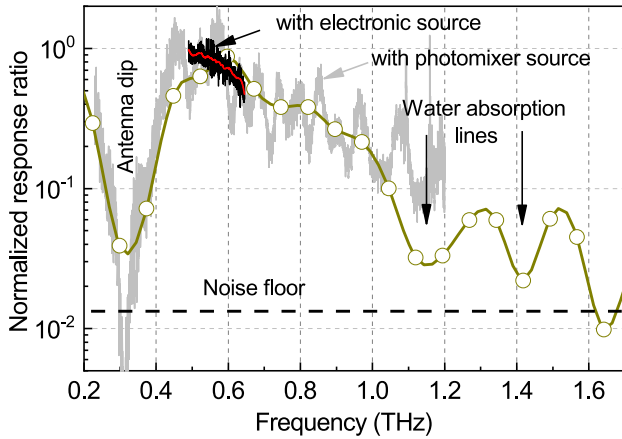


**Figure 5.** The ratio between TeraFET response and electro-optic recorded spectra (dark yellow line). The red line shows the detector's cw characterization with electronic source. The light grayed data in the background results from photomixer characterizations referenced to Golay cell detector. Strong modulations, which are seen in this data, result from standing waves in diamond window.

50 GHz to 1.2 THz and referenced against the Golay-cell detector with diamond window. All measurements show good agreement, confirming that the general slope of the performance loss over the frequency is a device characteristics. Such behavior was not expected by us (starting by the maximum of responsivity at 500 GHz, the device was designed to have only a 50% performance roll-off at 1.2 THz) and will be discussed in the forthcoming theory section.

Although the autocorrelation technique does not allow deducing internal times for the build-up of rectified signal in TeraFETs, the presence of the nonlinear dependency of the response allows concluding that the response is nearly instantaneous (for details see [18]), limited only by the speed of the employed read-out electronics. This statement can be supported by a theory [29, 31] which describes the transistor response to short pulses using a viscous hydrodynamic model for a gate-controlled 2DEG. Based on the aforementioned theory, we calculated the intrinsic response time of our AlGaIn/GaN HEMT, which resulted to about 50 fs (when the mobility is  $1013 \text{ cm}^2 \text{ V}^{-1} \text{ s}^{-1}$ , the channel length 100 nm and the gate voltage  $-0.95 \text{ V}$ ). Thus we speculate that the TeraFETs can be used in the observation of dynamic processes with a temporal resolution on the order of one picosecond such like the mode-locking processes of the THz quantum cascade lasers.

#### 4. TeraFET detector response theory

In order to analyze the measured roll-off of detector performance, we will revise the arguments of non-quasistatic theory of the detection.

##### 4.1. Intrinsic responsivity

The response of the TeraFET device can be treated in the framework of plasma wave mixing as it has been initially

proposed by Dyakonov and Shur [9] and further elaborated to account for nonlinear charge carrier density dependency on the gate voltage  $V_G$  in the vicinity of the threshold voltage  $V_{th}$  [4, 32], where such detectors typically show the best performance values. When the THz signal with its voltage amplitude  $V_{THz}$  is coupled to the two-dimensional electron gas in the channel of the field-effect transistor, it induces voltage response  $\Delta V$  which can be expressed as the product of a quasi-stationary transistor geometry and material related quantities and a frequency-dependent rectification efficiency factor  $f(\omega, \tau)$

$$\Delta V = \frac{q}{m^*} \frac{V_{THz}^2}{4s^2} \cdot f(\omega, \tau), \quad (2)$$

where  $m^*$  is the effective mass of electron,  $\tau$ —their momentum scattering time,  $q$ —the elementary charge,  $\omega$ —the radian frequency of the applied excitation signal and  $s$ —the velocity of plasma waves under the gate. In the scattering time approximation and for non-degenerate electron gas, the  $s$  can be calculated from the voltage dependency of the resistance (or conductance) of the gated part  $R_{ch}$ :

$$s = \sqrt{\frac{q}{m^*} \frac{1}{R_{ch}} \left( \frac{\partial}{\partial V_G} \frac{1}{R_{ch}} \right)^{-1}}. \quad (3)$$

The response can also be read-out as an induced current signal which relates induced voltage through the quasistatic drain-source resistance  $R_{DC}$  by a simple equation  $\Delta I = \Delta V/R_{DC}$ .

It is important to note, that the channel with impedance  $Z_{ch}$  excited by the amplitude  $V_{THz}$  will absorb a power

$$P_{in} = \frac{V_{THz}^2}{2} \frac{\text{Re}(Z_{ch})}{|Z_{ch}|^2}. \quad (4)$$

The intrinsic responsivity for current  $\mathfrak{R}_I$  (or voltage responsivity  $\mathfrak{R}_V$ ) relates the detector's radiation response to this absorbed power:

$$\mathfrak{R}_{I,in} = \frac{\Delta I}{P_{in}} = \frac{q}{2m^*s^2} \cdot \frac{1/R_{ch}}{\text{Re}(Z_{ch}^{-1})} \cdot f(\omega, \tau). \quad (5)$$

The first term  $q/(2m^*s^2)$  in this equation represents a quasistatic responsivity  $\mathfrak{R}_{I,QS}$  of the transistor. The second—represents a ratio between quasistatic and high-frequency admittances. It is worth to note that deep in the sub-threshold, where carrier density  $n$  has an exponential dependency on  $V_G - V_{th}$ , the  $\mathfrak{R}_{I,QS}$  approaches a diode-like responsivity  $q/(\eta_D k_B T)$ , where  $\eta_D$  represents ideality factor,  $k_B$  is the Boltzmann constant, and  $T$  is the temperature.

##### 4.2. Boundary conditions for the efficient rectification

Although plasma oscillations can form in fully symmetrically excited FET channels, no net measurable response to the incident radiation would build-up [33]. As a rule, efficient rectification can be achieved when one end (drain or gate) of the channel is subject to the full potential oscillation, while the other end (source) is pinned to AC ground. There are two main coupling schemes: the drain-source coupling and the gate-source coupling. For the drain-source coupling, which

requires a capacitive coupling between either gate-drain or gate-source terminals, the rectification efficiency factor takes the form:

$$f = 1 + \beta \cdot \frac{\sinh^2(\text{Im}(k)L_{\text{ch}}) - \sin^2(\text{Re}(k)L_{\text{ch}})}{\cosh^2(\text{Im}(k)L_{\text{ch}}) - \cos^2(\text{Re}(k)L_{\text{ch}})}, \quad (6)$$

here  $\beta = 2\omega\tau/\sqrt{1 + (\omega\tau)^2}$ . For the gate-source coupling,  $f$  can be expressed as

$$f = 1 + \beta - \frac{1 + \beta \cdot \cos(2\text{Re}(k)L_{\text{ch}})}{\sinh^2(\text{Im}(k)L_{\text{ch}}) + \cos^2(\text{Re}(k)L_{\text{ch}})}. \quad (7)$$

Here  $k$  is the plasmon wavevector

$$k = \frac{\omega}{s} \sqrt{1 + \frac{i}{\omega\tau}}. \quad (8)$$

The plasma wavevector in (8) is a complex quantity and hence, together with the length of the gated channel  $L_{\text{ch}}$ , describes propagation and attenuation of the waves [9]. For high frequencies  $\omega\tau \gg 1$ , the waves can oscillate multiple times before decaying. It is so-called plasmonic mixing regime. Furthermore, in a short channel ( $L_{\text{ch}} \leq s\tau$ ), the waves can reach channel's end and be reflected off the boundary before they are significantly attenuated. The channel then acts as a cavity for standing waves where superposition of waves and resonance features can evolve. In this case the detector works in so-called resonant plasmonic mixing regime.

When a transistor channel is comparatively long ( $L_{\text{ch}} \gg s\tau$ ), the waves get overdamped and do not reach the end of the channel. In this device operation regime both equations (6) and (7) approach to the same efficiency factor:

$$f \approx 1 + \beta = 1 + \frac{2\omega\tau}{\sqrt{1 + (\omega\tau)^2}}. \quad (9)$$

The mathematical treatment of high-frequency transport in 2DEG, in general, can be represented graphically in the form of a RLC transmission line with following elements: resistance  $R_i = (qn\mu W)^{-1}$ , inductance  $L_i = R_i\tau$ , and the capacitance  $C_i = qW\partial n/\partial V_G$  defined per unit of length, with  $\mu$  being the carrier mobility. It has been shown in the literature, that this approach can be useful solving various problems, including the modeling of TeraFET responsivity [34, 35] or the description of the evolution of the plasmonic band spectrum in plasmonic crystals [36].

Figure 6 displays the modeled rectification efficiency factors versus radiation frequency for an AlGaIn/GaN TeraFET which we use in the experimental part of this paper. Three enhancement factors are compared: for drain-coupling (red dotted lines), gate-source coupling (blue dashed), and the long-channel or the overdamped-plasmon limit case (black solid). Three different gate bias voltages are used in calculations: 0 V, at which the transistor is normally opened,  $-0.5$  and  $-0.95$  V which is near the threshold voltage. The last gate voltage was used in the autocorrelation part of the experiment (see section 3.2). The quasistatic (distributive resistive mixing approximation) limit of (9) is set by unity for drain-coupling and zero for gate-source coupling.

At low frequencies the transistor operates as a classical resistive mixer in the quasistatic limit of the two-dimensional

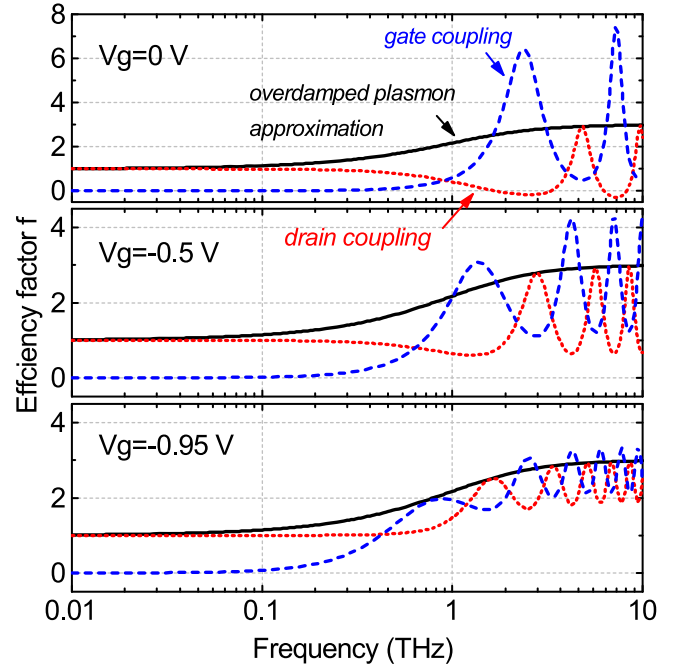


**Figure 6.** Plasmonic enhancement factors versus radiation frequency of an AlGaIn/GaN TeraFET used in autocorrelation experiments. The plot displays the enhancement factors for drain-coupling (red dotted lines), gate-source coupling (blue dashed) and the overdamped-plasmon limit (black solid) for three different gate bias voltages  $V_G$ .

electron gas response to the applied voltages. However at the high frequencies (above 100 GHz), this approximation has to be extended by the non-quasistatic treatment. The overdamped-plasmon approximation predicts enhancement ( $\times 3$ ) above 1 THz. Resonant features appear when plasma waves get reflected from the end of the channel. Depending on the coupling scheme, either resonances or anti-resonances appear at the multiples of fundamental cyclic resonance frequency  $\omega_0 = 2\pi s/(4L_{\text{ch}})$ . Figure 6 also clearly shows the major difference between the drain and the gate-source coupling schemes.

The frequencies for the resonance peak and their heights depend on both the coupling scheme and the applied voltage to the gate of HEMT transistor. The increase of gate voltage above the threshold lowers the channel resistance and, consequently, controls the position of resonance peak as can be mathematically traced with (3) and (8). This feature forms the basis for the efforts towards frequency-agile THz detectors [9, 37–39]. This concept, however, does not account neither for the intrinsically absorbed power, nor for the antenna coupling that might diminish the role of plasmonic resonances.

The impedance of the gated part of the transistor's channel depends on the exact boundary conditions. An analogy with the transmission line formalism allows for analytical representation via its characteristic impedance  $Z_0 = \sqrt{(R_i + i\omega L_i)/(i\omega C_i)}$  and an arbitrary load  $Z_L$ :

$$Z_{\text{ch}} = Z_0 \frac{Z_L + Z_0 \tanh(\gamma L_{\text{ch}})}{Z_0 + Z_L \tanh(\gamma L_{\text{ch}})}, \quad (10)$$

where the propagation constant  $\gamma = ik^*$ . Therefore, for

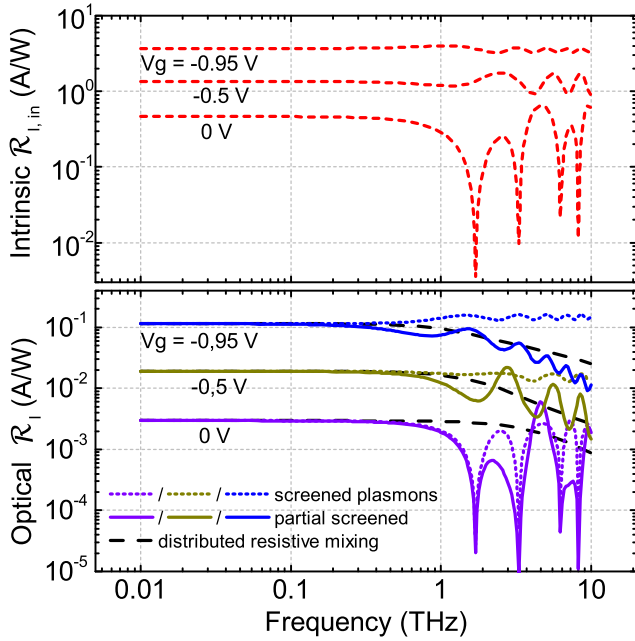


**Figure 7.** Responsivities versus radiation frequency of an AlGaIn/GaN TeraFET used in our experiment. The top figure displays the intrinsic responsivity (red short-dashed lines) according to (5); the bottom figure displays the optical responsivity calculated using (13) and for three different gate bias voltages  $V_G$ . Dotted lines correspond to the case of fully screened plasmons whereas solid lines account for partial screening and black dashed lines correspond to the distributed resistive mixing model.

previously discussed boundary conditions with AC short ( $Z_L = 0$ ) the channel impedance can be expressed as  $Z_{ch} = Z_0 \tanh(\gamma L_{ch})$  and for an AC-open case ( $Z_L = \infty$ ), the resulting impedance is  $Z_{ch} = Z_0 \coth(\gamma L_{ch})$ .

#### 4.3. The role of gate screening

Until now, the plasmons which get excited in the channel of the transistor by coupled radiation have been treated as fully screened by the gate electrode. This approximation is valid as long as plasmon wavelength is much longer than the distance  $d$  from the channel to the gate electrode, i.e.  $d \ll 2\pi/\text{Re}(k)$ . If this condition is not fulfilled, the equations for the impedance and the rectification efficiency must be revised. In the most general case, a three-dimensional Poisson equation should be solved together with standard charge continuity and transport equations. However, when the channel length  $L_{ch} \gg d$  and  $L_{ch} \ll W$ , a decoupled solution for electric fields in parallel and perpendicular to the channel directions can be assumed, reducing the solution to two one-dimensional tasks. The procedure has been initially used to model plasmons in graphene [40] or for the treatment of plasmonic crystals [41].

The simplification allows to employ relation between the Fourier component for statically screened Coulomb potential  $\varphi_1$  and the Fourier component of carrier density  $n_1$  applying a linear approximation for long wavelength plasmons (or small wavevectors  $k$ ) as used by [42]:

$$\varphi_1 = \frac{-qn_1}{2\epsilon_0\bar{\epsilon}(k+k_s)} \quad (11)$$

with the effective dielectric constant  $\bar{\epsilon} = (\epsilon_a + \epsilon_b)/2$  where  $\epsilon_a$  and  $\epsilon_b$  being dielectric constants of material above and below the 2DEG layer and the screening wavevector  $k_s = q^2/(2\epsilon_0\bar{\epsilon}) \cdot dn/dE_F$ ,  $\epsilon_0$  is the dielectric permittivity of vacuum and  $E_F$  is the Fermi energy. We would like to note, that the (11) differs from that used in [40, 41]. It does not include a finite distance  $d$  between the gate and the channel, but accounts the gate-induced charge. The later is of importance for the device operation in the vicinity of threshold voltage. The plasmon wavevector can be found from the solution of the following dispersion relation:

$$\omega^2 - i\frac{\omega}{\tau} - \frac{q^2k^2n}{2\epsilon_0\bar{\epsilon}m^*(k+k_s)} = 0. \quad (12)$$

The impedance of the channel can be found from (10) with only modification for the capacitance per unit of length which obtains a more general form  $C_i = 2\epsilon_0\bar{\epsilon}W(k+k_s)$ . In this case, the propagation constant is calculated from  $\gamma = \sqrt{i\omega C_i(R_i + i\omega L_i)}$ .

#### 4.4. Device responsivity

The transistor's optical performance is always reduced compared to the intrinsic case due to inevitable loss of RF power absorption, RF power distribution over intrinsic transistor and the parasitic elements such as shunting capacitances and series resistors, and the impedance mismatch. Thus the device current responsivity can be approximated as follows:

$$\mathfrak{R}_I = \mathfrak{R}_{I,in} \cdot \eta \cdot M \cdot H_P. \quad (13)$$

The  $\eta$  comprises modeled antenna efficiency as well as optical loss due to reflections and Gaussian beam coupling,  $M$  is the power matching factor, describing the impedance mismatch between the antenna feed-point impedance  $Z_{ant}$  and the transistor impedance. The  $H_P$  is the power distribution between the channel and the ungated transistor part together with the ratio between the resistance of the equivalent current source and the total DC resistance. For a typical HEMT when the influence of the shunting capacitance is negligible comparing with the role of in-series connected resistance  $R_{ug}$ , both factors can be expressed with following representations:

$$M = \frac{4\text{Re}(Z_{ch} + R_{ug})\text{Re}(Z_{ant})}{|Z_{ch} + R_{ug} + Z_{ant}|^2}, \quad (14)$$

$$H_P = \frac{R_{ch}}{R_{DC}} \cdot \frac{\text{Re}(Z_{ch})}{\text{Re}(R_{ug} + Z_{ch})}. \quad (15)$$

In many FET technologies, the transistor channel is only partially gated and embedded in ungated access regions. The carrier density-controlling function of the gate metal has no impact on these regions where a fixed carrier density exists. The ungated channel regions therefore constitute a gate voltage-independent series resistance to the total drain-source resistance of the device. Here we assume, that ungated regions do not contribute directly to the plasma wave-based detection mechanism, however, if the transistor is biased to the deep inversion, these parasitic elements can also influence on the performance of detector [27, 43, 44].



Finally, the noise equivalent power (NEP) of the detector can be derived as

$$\text{NEP} = \frac{\sqrt{4k_B T}}{\sqrt{R_{\text{DC}} \mathfrak{R}_I}} = \frac{\sqrt{4k_B T R_{\text{DC}}}}{\mathfrak{R}_V}. \quad (16)$$

For FET detector without applied drain bias, the dominant noise source is thermal Johnson–Nyquist noise. This also has been experimentally verified for the AlGaIn/GaN, AlGaAs/GaAs, CMOS and graphene transistor-based detectors [45].

Figure 7 shows simulations of ‘intrinsic’ and optical device responsivities for the drain-coupling scheme. The AlGaIn/GaN transistor is the same as used for a modeling of  $f(\omega, \tau)$ . Since the optical responsivity requires including specific antenna, for simulations we used the analytical prediction based on Babinet principle for the ideal bow-tie antenna with  $60^\circ$  angle for metal leafs on semi-infinite dielectric with  $\epsilon = 9.7$ , i.e.  $Z_{\text{ant}} \approx 100 \Omega$ .

Figure 7 also indicates that no significant enhancement of detection sensitivity can be expected in resonant plasmonic detector operation regime of TeraFET operation. The sharper resonant spikes can be seen only in the transistor which gate voltage is far from the threshold (violet lines) where the sensitivity of detectors is much lower compared with the optimum sensitivity.

The simulation of a broadband bow-tie antenna which has been used for our detector shown nearly constant efficiency of 36% in the 0.4–2 THz range. In addition, in factor  $\eta$  we include 30% reflection at the surface of hyperhemispheric Si lens and a fixed factor of 0.8 for Gaussian beam coupling efficiency. At 500 GHz, modeled optical responsivity corresponds very well with experimentally measured  $100 \text{ mA W}^{-1}$  and  $30 \text{ pW Hz}^{-1/2}$ , thus validating model parameters. However, standard distributed transmission line theory fails to predict experimentally observed frequency roll-off shown in the figure 5. This roll-off can be explained if the responsivity would be calculated with the impedance estimation for partially gated plasmons and the distributed resistive mixing model (without plasmonic contribution) represented with solid and black dashed curves, respectively, in the lower part of the figure 7. Indeed, for the gate bias voltage of  $-0.95 \text{ V}$ , the equality between the screening wavenumber and the gated plasmon wavenumber is expected at about 770 GHz.

For the moment, there is no rigorous theory which would describe mixing efficiency factor in the case of changing dispersion law (from instead of form screened to partially-screened by the gate electrode). Therefore, we used unmodified efficiency formula for drain-source coupling conditions given by the (6). The prediction for a roll-off comes directly from the decreasing real part of the impedance which otherwise oscillates around the constant value. It is interesting to note, that the result very closely resembles predictions of device theory which omits the plasmonic contribution [46]. Similar discrepancy between the plasmon-based theory predictions and the experimentally measured stronger roll-off is reported for AlGaAs/GaAs HEMTs [47]. Contrary to this, a remarkable agreement between the broadband measurements and the screened-plasmon approximation theory was obtained

for detectors implemented in 90 nm CMOS technology [19] where gate-to-channel separation is only about 2.5 nm (resulting to several times larger screening wavenumber). Therefore, we would like to conclude, that our findings are important for the design of novel devices, which intend to exploit plasmon-specific properties disregarding of material system: either for high-electron mobility III/V-devices or graphene, the gate-to-channel separation must be intentionally reduced in order to follow predictions made using a screened-plasmon approximation. This conclusion goes along the same line as for increasing the threshold frequency of field-effect transistors [48].




## 5. Conclusions

We showed that AlGaIn/GaN TeraFETs can efficiently detect the sub-picosecond THz pulses generated by a high repetition rate infrared laser and an ultrafast large-area interdigitated photoconductive antenna. The photoresponse of our TeraFET proved to be linear—with respect to radiation power—in a wide range of a bias gate voltages and intensities reaching up to hundreds of milliwatts in a peak power. We demonstrated that the achieved system SNR ( $\sim 20 \text{ dB}$ ) of our TeraFET allows the implementation of an autocorrelation measurement technique and opening the possibility of spectral characterization of pulsed THz sources. Furthermore, the frequency response of the TeraFET could be studied within a bandwidth exceeding 1 THz. In our measurements, we experimentally observed a performance roll-off which cannot easily be predicted using a framework of standard distributed transmission line theory. Therefore, we proposed to include other factors like the dispersion of a transition from screened to unscreened plasmons as an extension of the common detection theory. Finally, we conclude that for novel detectors and radiation sources, which intend to utilize plasma waves, it is important to ensure a much longer screening wavenumber than the wavevector of the involved plasmon.

## Acknowledgments

The Research Council of Lithuania is gratefully acknowledged for the financial support under Contract No. S-LAT-17-3. The Frankfurt team thanks the European Union’s Horizon 2020 research and innovation program for the Grant Agreement No. 675683 (CELTA).

## ORCID iDs

A Lisauskas  <https://orcid.org/0000-0002-1610-4221>  
 D Čibiraitė  <https://orcid.org/0000-0002-1949-6312>  
 H G Roskos  <https://orcid.org/0000-0003-3980-0964>

## References

- [1] Preu S, Mittendorff M, Winnerl S, Cojocari O and Penirschke A 2015 *IEEE Trans. Terahertz Sci. Technol.* **5** 922–9
- [2] Mittendorff M, Winnerl S, Kamann J, Eroms J, Weiss D, Schneider H and Helm M 2013 *Appl. Phys. Lett.* **103** 021113
- [3] Bauer M, Rämmer A, Boppel S, Chevtchenko S, Lisauskas A, Heinrich W, Krozer V and Roskos H G 2015 High-sensitivity wideband THz detectors based on GaN HEMTs with integrated bow-tie antennas *Proc. 10th European Microwave Integrated Circuits Conf. (EuMIC)* (Paris: IEEE) pp 1–4
- [4] Boppel S *et al* 2012 *IEEE Trans. Microw. Theory Tech.* **60** 3834–43
- [5] Romeo L, Coquillat D, Pea M, Ercolani D, Beltram F, Sorba L, Knap W, Tredicucci A and Vitiello M S 2013 *Nanotechnology* **24** 214005
- [6] Vicarelli L, Vitiello M S, Coquillat D, Lombardo A, Ferrari A C, Knap W, Polini M, Pellegrini V and Tredicucci A 2012 *Nat. Mater.* **11** 865–71
- [7] Zak A, Andersson M A, Bauer M, Matukas J, Lisauskas A, Roskos H G and Stake J 2014 *Nano Lett.* **14** 5834–8
- [8] Bandurin D A, Gayduchenko I, Cao Y, Moskotin M, Principi A, Grigorieva I V, Goltsman G, Fedorov G and Svinsov D 2018 *Appl. Phys. Lett.* **112** 141101
- [9] Dyakonov M and Shur M 1996 *IEEE Trans. Electron Devices* **43** 380–7
- [10] Bauer M, Andersson M, Zhang J, Sakalas P, Čibiraitė D, Lisauskas A, Schröter M, Stake J and Roskos H G 2015 *J. Phys.: Conf. Ser.* **647** 012004
- [11] Bauer M, Boppel S, Zhang J, Rämmer A, Chevtchenko S, Lisauskas A, Heinrich W, Krozer V and Roskos H G 2016 *Int. J. High Speed Electron. Syst.* **25** 1640013
- [12] Bauer M *et al* A high-sensitivity AlGaIn/GaN HEMT terahertz detector with integrated broadband bow-tie antenna unpublished
- [13] Preu S, Mittendorff M, Winnerl S, Lu H, Gossard A C and Weber H B 2013 *Opt. Express* **21** 17941
- [14] Lisauskas A *et al* 2014 *J. Infrared, Millim., Terahertz Waves* **35** 63–80
- [15] But D B, Drexler C, Sakhno M V, Dyakonova N, Drachenko O, Sizov F F, Gutin A, Ganichev S D and Knap W 2014 *J. Appl. Phys.* **115** 164514
- [16] Dyakonova N *et al* 2015 *Opto-Electron. Rev.* **23** 195–9
- [17] Dyakonova N, Faltermeier P, But D B, Coquillat D, Ganichev S D, Knap W, Szkudlarek K and Cywinski G 2016 *J. Appl. Phys.* **120** 164507
- [18] Lisauskas A *et al* 2018 *APL Photonics* **3** 051705
- [19] Ikamas K, Čibiraitė D, Lisauskas A, Bauer M, Krozer V and Roskos H G 2018 *IEEE Electron Device Lett.* **39** 1413–6
- [20] Baillergeau M, Maussang K, Nirrengarten T, Palomo J, Li L H, Linfield E H, Davies A G, Dhillon S, Tignon J and Mangeney J 2016 *Sci. Rep.* **6** 24811
- [21] Hale P J, Madeo J, Chin C, Dhillon S S, Mangeney J, Tignon J and Dani K M 2014 *Opt. Express* **22** 26358
- [22] Dreyhaupt A, Winnerl S, Dekorsy T and Helm M 2005 *Appl. Phys. Lett.* **86** 121114
- [23] Siebert K J, Lisauskas A, Löffler T and Roskos H G 2004 *Japan. J. Appl. Phys.* **43** 1038–43
- [24] Loata G C, Thomson M D, Löffler T and Roskos H G 2007 *Appl. Phys. Lett.* **91** 232506
- [25] Preu S, Kim S, Verma R, Burke P G, Sherwin M S and Gossard A C 2012 *J. Appl. Phys.* **111** 024502
- [26] Khmyrova I and Seijyou Y 2007 *Appl. Phys. Lett.* **91** 143515
- [27] Lisauskas A, Bauer M, Rämmer A, Ikamas K, Matukas J, Chevtchenko S, Heinrich W, Krozer V and Roskos H G 2015 Terahertz rectification by plasmons and hot carriers in gated 2d electron gases *Proc. 41st Int. Conf. Noise and Fluctuations (ICNF)* (IEEE) pp 1–5
- [28] Gutin A, Kachorovskii V, Muraviev A and Shur M 2012 *J. Appl. Phys.* **112** 014508
- [29] Rudin S, Rupper G, Gutin A and Shur M 2014 *J. Appl. Phys.* **115** 064503
- [30] Maussang K *et al* 2017 *Appl. Phys. Lett.* **110** 141102
- [31] Rudin S, Rupper G and Shur M 2015 *J. Appl. Phys.* **117** 174502
- [32] Knap W *et al* 2002 *J. Appl. Phys.* **91** 9346
- [33] Boppel S *et al* 2016 *IEEE Trans. Terahertz Sci. Technol.* **6** 348–50
- [34] Lisauskas A, Pfeiffer U, Öjefors E, Bolivar P H, Glaab D and Roskos H G 2009 *J. Appl. Phys.* **105** 114511
- [35] Sakhno M, Golenkov A and Sizov F 2013 *J. Appl. Phys.* **114** 164503
- [36] Dyer G C, Aizin G R, Preu S, Vinh N Q, Allen S J, Reno J L and Shaner E A 2012 *Phys. Rev. Lett.* **109** 126803
- [37] Knap W, Deng Y, Rummyantsev S, Lü J Q, Shur M S, Saylor C A and Brunel L C 2002 *Appl. Phys. Lett.* **80** 3433–5
- [38] El Fatimy A *et al* 2006 *Appl. Phys. Lett.* **89** 131926
- [39] Tonouchi M 2007 *Nat. Photon.* **1** 97–105
- [40] Rana F 2008 *IEEE Trans. Nanotechnol.* **7** 91–9
- [41] Aizin G R and Dyer G C 2012 *Phys. Rev. B* **86** 235316
- [42] Ando T, Fowler A and Stern F 1982 *Rev. Mod. Phys.* **54** 437
- [43] Shur M 2010 *Electron. Lett.* **46** S18
- [44] Popov V V, Koudymov A N, Shur M and Polischuk O V 2008 *J. Appl. Phys.* **104** 024508
- [45] Čibiraitė D, Bauer M, Rämmer A, Chevtchenko S, Lisauskas A, Matukas J, Krozer V, Heinrich W and Roskos H G 2017 Enhanced performance of algan/gan hemt-based thz detectors at room temperature and at low temperature *Proc. 42nd Int. Conf. on Infrared, Millimeter, and Terahertz Waves (IRMMW-THz)* pp 1–2
- [46] Sizov F, Sakhno M, Golenkov A, Petryakov V, Tsybrii Z, Reva V and Zabudsky V 2014 Uncooled rectification and bolometer type THz/Sub-THz detectors *THz and Security Applications* ed C Corsi and F Sizov (Dordrecht: Springer) pp 53–73
- [47] Regensburger S, Mukherjee A k, Schonhuber S, Kainz M A, Winnerl S, Klopff J M, Lu H, Gossard A C, Unterrainer K and Preu S 2018 *IEEE Trans. Terahertz Sci. Technol.* **8** 465–72
- [48] Kim D H, Brar B and del Alamo J A 2011  $f_T = 688$  GHz and  $f_{max} = 800$  GHz in  $l_g = 40$  nm  $In_{0.7}Ga_{0.3}As$  MHEMTs with  $g_{m,max} = 2.7$  mS/ $\mu m$  2011 *IEEE Int. Electron Devices Meeting (IEDM)* (IEEE) pp 13–6